Enhanced carriers' separation and transport with ferroelectric polymer P(VDF-TrFE) in hole-transporting material free carbon based perovskite solar cells

H. J. Tao[a,b*], Z. T. Chen[a], M. Q. Wang[a], C. X. Zhang[c], W. J. Zhang[a], L. L. Ding[a], J. W. Li[a], X. Q. Li[a]

[a]*Jiangsu Key Laboratory of Materials and Technology for Energy Conversion, College of material science and technology, Nanjing University of Aeronautics and Astronautics, Nanjing 211100, PR China*

[b]*Jiangsu Collaborative Innovation Center of Photovoltaic Science and Engineering, Changzhou University, Changzhou 213164, Jiangsu, PR China*

[c]*College of Materials Engineering, Nanjing Institute of Technology, Nanjing 211167, PR. China*

The separation and transport of carriers is the key to improve the efficiency of the hole transport material free carbon based perovskite solar cells (C-PSCs). Here, ferroelectric polymer P(VDF-TrFE), which is doped into $CH_3NH_3PbI_3$ layer and inserted as the interface layer between TiO_2 and $CH_3NH_3PbI_3$ layers as well, is adopted to achieve this goal. For one thing, P(VDF-TrFE) improves the crystallinity of perovskite films, leading to lower defects and reducing carriers' recombination. For the other thing, the built-in field of C-PSCs is enhanced due to the existence of polarized P(VDF-TrFE) when the external voltage is applied to the device, which effectively promotes the transport of carriers at TiO_2/$CH_3NH_3PbI_3$ interface. Finally, a high short-circuit current density of 16.25 mA/cm^2 is obtained with a power conversion efficiency of 7.83% for the optimal C-PSCs based on the polarized TiO_2/P(VDF-TrFE)/$MAPbI_3$:P(VDF-TrFE). Meanwhile, the hysteresis of the device is reduced as well. This simple and effective method is conducive to the commercialization of C-PSCs in the future.

(Received November 12, 2021; Accepted February 22, 2022)

Keywords: Separation and transport of carriers, Perovskite solar cells, P(VDF-TrFE), Crystallinity, Built-in field

1. Introduction

Much The hole transport material free carbon-based perovskite solar cells (C-PSCs) has been considered as one of the candidates for commercial perovskite solar cells, due to its excellent stability and lower cost [1]. However, to date the highest power conversion efficiency (PCE) of C-PSCs is only 16.37% [2], which is far lower than the current record of 25.2% in traditional

* Corresponding author: taohaijun@nuaa.edu.cn
https://doi.org/10.15251/DJNB.2022.171.247

perovskite solar cells (PSCs) [3]. Therefore, improving the PCE of C-PSCs has become an urgent task. The electron-transporting layer (ETL)/perovskite interface, as the only region of effective carriers' separation and transport [4], is critical to the improved performance of C-PSCs.

In order to improve the separation and transport of carriers, many efforts have been made. TiO_2 is the most common materials of ETL. However, many surface defects exist in TiO_2 ETL as well as low carrier mobility, leading to hindering the fast transport of photo-generated electrons in the ETL/perovskite interface [5-7]. To solve these problems, attempts have been implemented, such as other TiO_2 nanostructures [8,9], elements doped TiO_2 and metal oxide passivation [10]. Although interface defects are passivated and the electrons extraction of TiO_2 ETL is improved, additional complex process and high temperature annealing not only increase cost but also are not suitable for commercialization of C-PSCs. Interface modification, a simple and feasible method, has been widely used for improving TiO_2 ETL [11]. Especially, self-assembled monolayer, which can tune the energy band structure of ETL/perovskite layers due its inherent dipole moment, has been an effective alternative to enhance the separation and transport of carriers at interface [12]. For example, an organic silane self-assembled monolayer is inserted between TiO_2 and perovskite to modify the TiO_2 ETL in C-PSCs [13]. While improving the interface contact, its molecular dipole can optimize interface band alignments, thus promoting the carriers transport at $TiO_2/CH_3NH_3PbI_3$ interface. Similarly, PCNN-3N-3I with a strong molecular electric dipole is also inserted into ETL/perovskite interface, which forms a dipole interlayer to reconfigure interfacial energy band structure, resulting in the improved separation and transport of carriers [14]. Therefore, the dipole interlayer existed in ETL/perovskite interface contributes to the carriers' separation and transport at interface. Ferroelectric materials can produce directional dipole array after polarization treatment due to its intrinsic characteristics, which makes it possible to use ferroelectric materials as modified layers in PSCs.

The application of ferroelectric materials in solar cells has been reported in literatures [15-17], in which the depolarization electric field induced by ferroelectric materials effectively promotes carriers transport. As for PSCs, ferroelectric $PbTiO_3$ and $BaTiO_3$ were firstly used to replace TiO_2 ETL, but low PCE was obtained after polarization treatment [18]. Subsequently, ferroelectric $Pb(Zr,Ti)O_3$ and $PbTiO_3$ were respectively used as ETL [19]. After polarization treatment, polarized $Pb(Zr,Ti)O_3$ and $PbTiO_3$ ETL show good carriers transport performance. And first principle calculation shows that polarized ferroelectric materials can provide effective electron extraction and inhibit the recombination of photo-generated carriers, so as to adjust the photocurrent density [20]. Especially, Yang et al [21] prepared the ultra-thin $PbTiO_3$ interface layer on TiO_2 surface in situ. Polarized $PbTiO_3$ interface layer effectively improved the separation and transport of carriers at interface and the PCE of prepared C-PSCs was more than 16%, which is the highest efficiency of C-PSCs at present. In addition to inorganic ferroelectric materials, organic ferroelectric P(VDF-TrFE) is also used in C-PSCs [22]. The results show that the perovskite film with polarized P(VDF-TrFE) doped has improved quality and enhance built-in field. Furthermore, the P(VDF-TrFE) interface depole layer inserted between perovskite and hole-transporting layers was helpful to the hole transport at interface, so as to improve the cells' performance [23].

Considering that inorganic ferroelectric materials need to be prepared at high temperature, this work introduces the organic ferroelectric P(VDF-TrFE), which can be prepared by low temperature solution method, into C-PSCs to improve the separation and transport of carriers at

$TiO_2/CH_3NH_3PbI_3$ interface. Firstly, $CH_3NH_3PbI_3$ with P(VDF-TrFE) doped is studied. Subsequently, P(VDF-TrFE) is inserted into $TiO_2/CH_3NH_3PbI_3$ interface. The concentration and polarization voltage of P(VDF-TrFE) ferroelectric interface layer are investigated. Finally, based on these, the structure of FTO/TiO_2/P(VDF-TrFE)/$CH_3NH_3PbI_3$:P(VDF-TrFE)/C is successfully built with P(VDF-TrFE) doped and used as interface layer. The separation and transport of carriers at $TiO_2/CH_3NH_3PbI_3$ interface are effectively improved in C-PSCs and higher PCE is obtained. This simple and efficient method provides a practical way to improve the performance of C-PSCs.

2. Experimental procedure

2.1. Device fabrication

To Fluorine-doped tin oxide conducting glass (FTO, Pilkington, thickness 2.2 mm, sheet resistance 8 Ω/square) is used as cells' substrate and cleaned by detergent solution, ethanol and distilled water for 15 min in an ultrasonic bath, respectively. Then the glasses are rinsed with distilled water, ethanol sequentially and dried in a drying oven. A compact layer of TiO_2 is deposited on the FTO substrates by spin-coating the titanium precursor solution at 2,000 rpm for 60 s, followed by annealing at 500 °C for 30 min. A mesoscopic TiO_2 layer is spin-coated on the compact layer and annealed at 500 °C for 30 min. Then the substrate is immersed in the $TiCl_4$ aqueous solution for 30 min at 70 °C and annealed at 500 °C for 30 min.

After that, a ferroelectric layer is deposited on the ETL by spin-coating the P(VDF-TrFE) solution which P(VDF-TrFE) powder is added to the DMF solution and stirred until clarified, at 3000 rpm for 60 s, followed by annealing at 100 °C for 60 min. The $CH_3NH_3PbI_3$ layer is fabricated through a one-step method: 1.2 mmol PbI_2 is mixed with 1.2 mmol MAI in the mixture solvent of 1 mL DMF:DMSO (915:85,v/v) for the preparation of perovskite precursor solution. In order to achieve ferroelectric doping, different amounts of DMF solution with 0.5 wt% P(VDF-TrFE) has substituted for the same amount DMF solution. The $MAPbI_3$ layer is deposited on the ferroelectric layer by spin-coating the perovskite precursor solution at 4000 rpm for 20 s, followed by annealing at 100 °C for 30 min. Finally, the as-prepared carbon slurry is doctor-bladed on the top of $MAPbI_3$ film, and followed by annealing at 100 °C for 60 min. All devices are assembled in a drying box, which can only control the humidity (10%-15%).

2.2. Characterization

An aqueous solution prepared using 0.02 M $TiOSO_4$, was dissolved in 0.03M of H_2O_2 and 0.1M KNO_3, and a few drops of 0.5M nitric acid were added to maintain pH = 1.6 at ambient temperature [19], the non-commercial fluorine-doped tin oxide (FTO) electrode [1], which served as the working electrode, a platinum Pt wire served as the counter electrode (CE) and a Saturated calomel electrode (ECS) was used as a reference. The deposition times were 60 min, under potentiostatic condition in the solution cited above, a bias voltage E = -1 V was applied at room temperature.

3. Results and discussion

In our study, the organic ferroelectric P(VDF-TRFE) is introduced into perovskite as an additive, and inserted as an interface dipole layer between the electron transport layer and the light absorption layer as well, to assemble the C-PSCs with FTO/TiO_2/P(VDF-TrFE)/ $MAPbI_3$:P(VDF-TrFE) /C structure. All the C-PSCs are assembled in a drying box (moisture about 10% - 15% RH) and texted outside without any encapsulation. In order to further improve the device performance, a polarization process is applied subsequently as the Fig.1 shows: an additional voltage is applied to the FTO substrate (FTO/TiO_2/P(VDF-TrFE)/ $MAPbI_3$:P(VDF-TrFE)), while a 10 μm polytetra-fluoroethylene (PTFE) film is inserted between the FTO substrate and an additional top FTO to avoid breakdown.

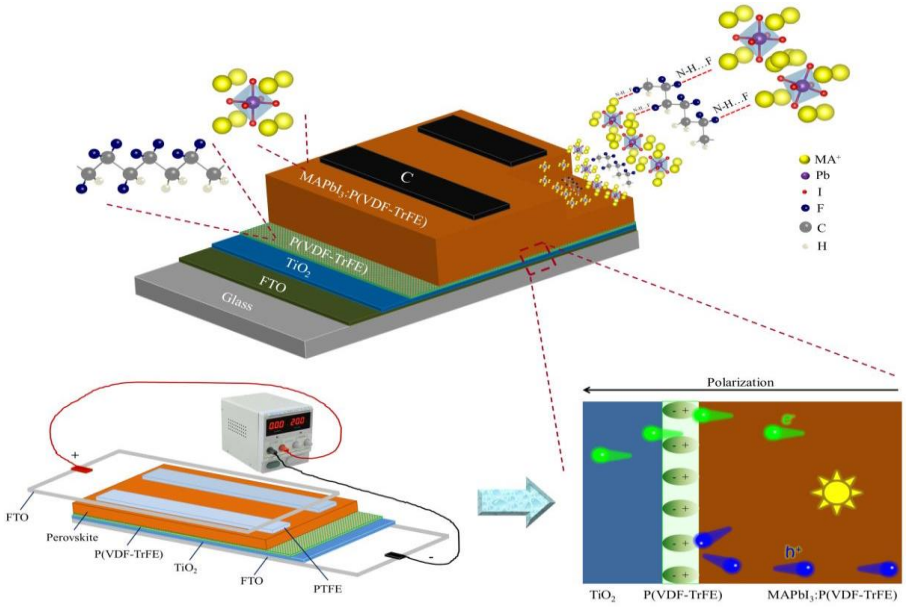

Fig. 1. Device configuration of the C-PSCs based on the TiO_2/P(VDF-TrFE)/ $MAPbI_3$:P(VDF-TrFE), schematic diagram of the polarization process, and the separation and transport of carriers. The P(VDF-TrFE) is doped in $MAPbI_3$ and/or inserted in TiO_2 and $MAPbI_3$ layers as the dipole layer. The polarization treatment is realized by applied an external voltage through the insertion of a 10 um polytetrafluoroethylene (PTFE) film between FTO substrate and an additional top FTO to avoid breakdown.

Firstly, to investigate the effect of P(VDF-TrFE) additive on the crystal structure of $MAPbI_3$ film, XRD patterns are performed, as shown in Fig.2.b. The perovskite film mainly contains the characteristic peaks of $MAPbI_3$ in consistent with the literature report [24], which indicates the addition of P(VDF-TrFE) will not change the crystal structure of $MAPbI_3$ film. What's more, it is found that the characteristic peak of the (110) crystal surface (14.02°) of $MAPbI_3$ was slightly enhanced (as shown in the red dotted line area) with the addition of P(VDF-TrFE) additive, indicating that the P(VDF-TrFE) additive could improve the crystallinity of $MAPbI_3$ film. The full width at half maximum (FWHM) of the (110) grain surface decreased

from 0.287 to 0.274, meaning the increase of corresponding grain size, which indicates that the P(VDF-TRFE) additives could increase the grain size of $MAPbI_3$. As Yang et al [22] reported, the F atoms in P(VDF-TrFE) can form NH...F hydrogen bonds with the H atoms in $MAPbI_3$, which slows down the transition from MA^+ to $MAPbI_3$, increases the crystal grains, improves film crystallinity, and improves film quality.

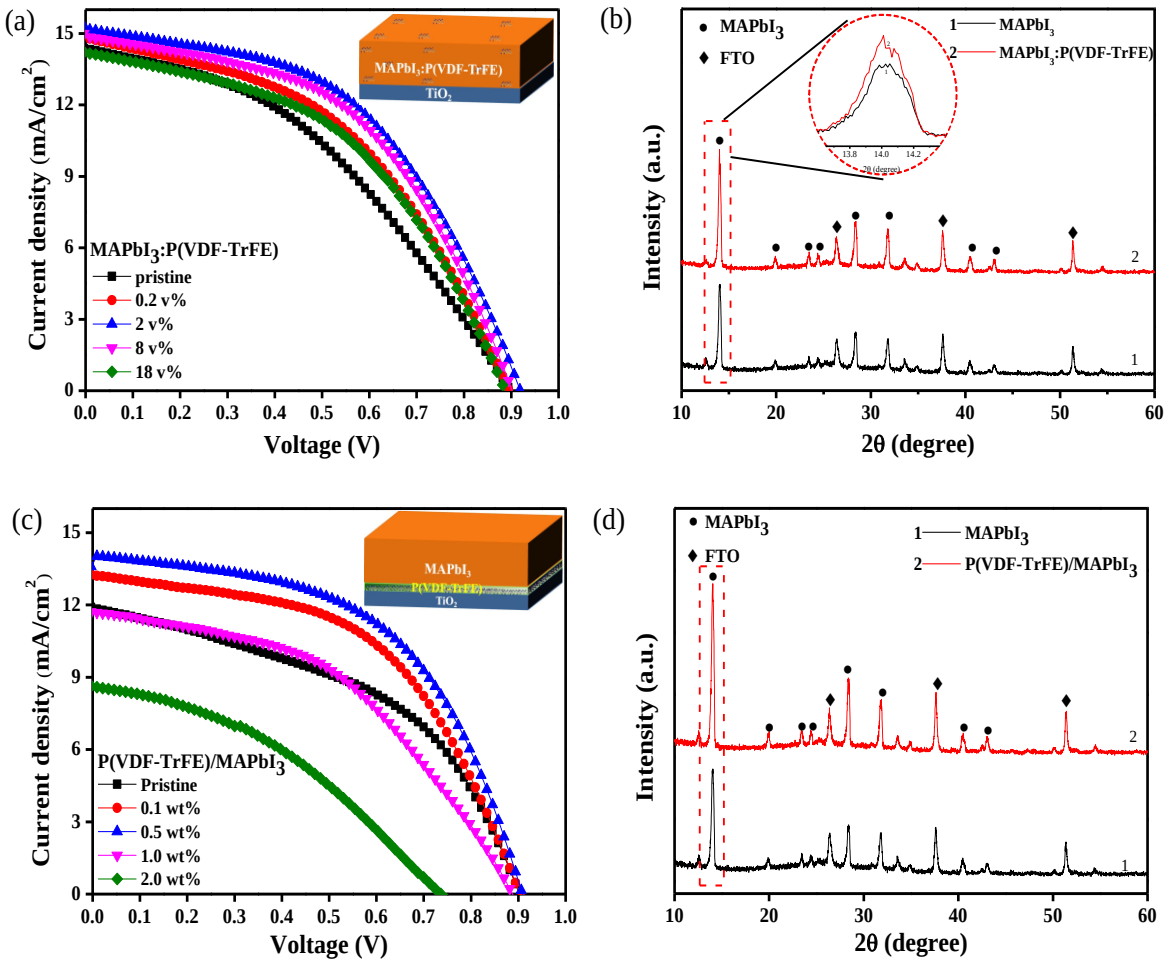

Fig. 2. a, b) J-V curves and XRD patterns in C-PSCs based the TiO_2/$MAPbI_3$:P(VDF-TrFE) dependent on different doping amount. c, d) J-V curves and XRD patterns in C-PSCs based the TiO_2/P(VDF-TrFE)/$MAPbI_3$ dependent on varied concentration.

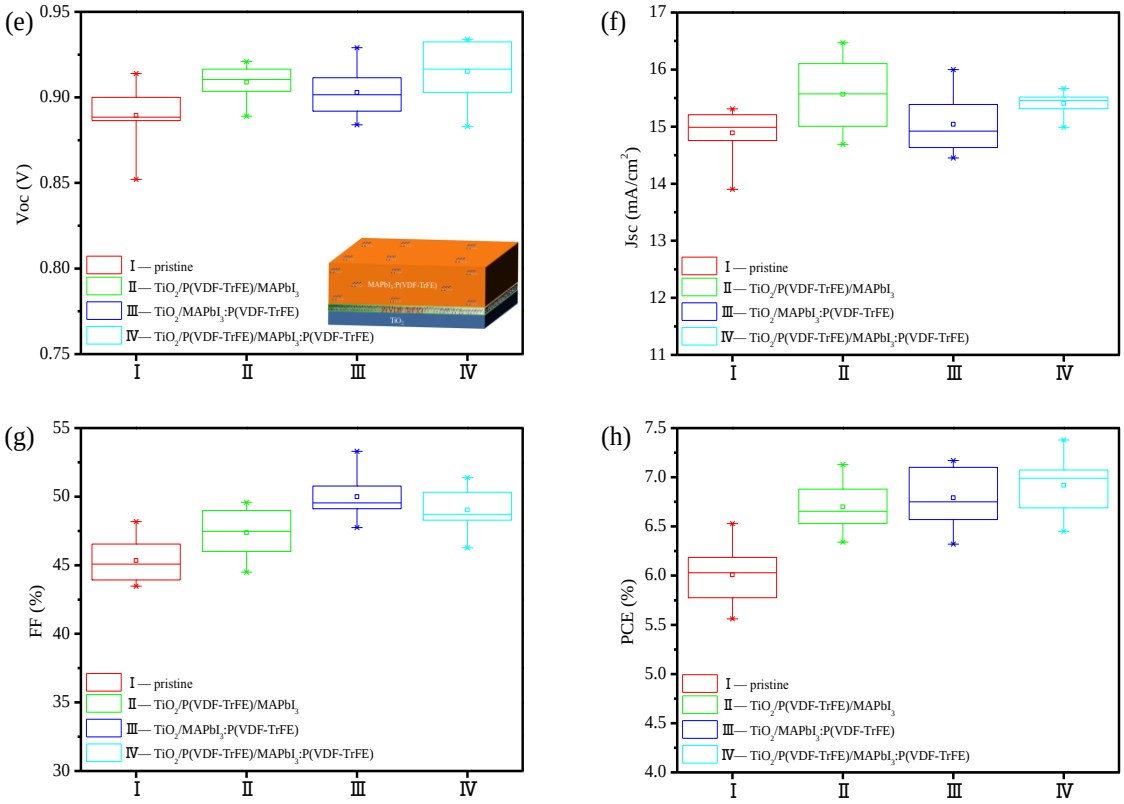

Fig. 2. e-h) The statistic performance parameters of the C-PSCs based on the TiO_2/$MAPbI_3$, TiO_2/$MAPbI_3$:P(VDF-TrFE), TiO_2/P(VDF-TrFE)/$MAPbI_3$ and TiO_2/P(VDF-TrFE)/$MAPbI_3$:P(VDF-TrFE).

Meanwhile, aim to study the effect of the addition amount of P(VDF-TrFE) in $MAPbI_3$ film on the device, the photoelectric properties measurements is tested after the C-PSCs with the pristine structure (FTO/TiO_2/$MAPbI_3$/C, recorded as devices-I) and the second structure (FTO/TiO_2/$MAPbI_3$:P(VDF-TrFE)/C, recorded as devices-II) is assembled. As shown in Fig.2.a, it can be seen that with the increase of P(VDF-TrFE) addition, the performance of the device firstly increases and then decreases. While the volume ratio reaches 2 v%, the device achieve the best performance. From the XRD spectroscopy of $MAPbI_3$ film, the main reason for the improved cell performance is the F-H bonds formed by F atoms in P(VDF-TrFE) and H atoms in $MAPbI_3$, slow down the crystallization process of $MAPbI_3$ to increases the grain size and crystallinity, thus improving the light absorption properties of the $MAPbI_3$ film and increasing the Jsc. However, due to the well insulation of P(VDF-TrFE), which harm to the charge transfer of the device, when P(VDF-TrFE) is added in large amounts (18 v%), Jsc decreases significantly and device performance deteriorates.

Secondly, the effect of P(VDF-TrFE) interfacial dipole layer on the crystal structure of $MAPbI_3$ film is investigated. As the analysis of XRD patterns shows (Fig.2.d), the P(VDF-TrFE) interfacial layer incapably change the crystal structure of $MAPbI_3$ film. In addition, the relative intensity ratio of (110) to (220) crystal plane of $MAPbI_3$ in the TiO_2/P(VDF-TrFE)/$MAPbI_3$ structure is 2.41, which is higher than that of the original sample. The intensity ratio is 2.41, which is higher than that of 2.34 in the original sample, indicating that the crystallinity of $MAPbI_3$ films

have been enhanced due to the existence of P(VDF-TrFE) interfacial layer. Meanwhile, the FWHM of $MAPbI_3$ film in the TiO_2/P(VDF-TrFE)/$MAPbI_3$ structure is 0.275, which is lower than that of 0.287 in the original sample, manifesting that the increase of the crystallinity and the grain size of $MAPbI_3$ film. From the above, it is clear that the increase of the crystallinity of $MAPbI_3$ film is related to the NH...F hydrogen bonds. However, due to the strong affinity of PbI_2 in DMF, the presence of high concentration of PbI_2 in the solution prevents the dissolution of P(VDF-TrFE) in DMF [23]. Therefore, it can be speculated that: the F atoms on the upper surface of the P(VDF-TrFE) interfacial layer form N-H...F hydrogen bonds with the H atoms in MA^+ in the lower surface of $MAPbI_3$ films, which retards crystallization of $MAPbI_3$, ultimately leading to the improvement of the $MAPbI_3$ film quality.

Similarly, in order to investigate the effect of the P(VDF-TrFE) interfacial dipole layer on the devices performance, C-PSCs with the third structure (FTO/TiO_2/P(VDF-TrFE)/$MAPbI_3$/C, recorded as devices-III) have been prepared. Fig.2.c shows the J-V curves of C-PSCs prepared with different P(VDF-TrFE) precursor concentrations, the devices perform best when the P(VDF-TrFE) precursor concentration is 0.5 wt%, indicating that the P(VDF-TrFE) film conduces to improve the devices performance, which as the result of the improvement of film quality and light-absorbing properties of $MAPbI_3$ layers.

Having said all of above, the devices with the fourth structure (FTO/TiO_2/P(VDF-TrFE)/$MAPbI_3$:P(VDF-TrFE)/C, recorded as devices-IV) is assembled. As the Fig.2.e-h shows, it can be found that devices-IV has the highest Voc, manifesting the lowest composite loss, which is mainly due to the dual passivation effect of the P(VDF-TrFE) doping and the P(VDF-TrFE) interfacial layer. However, the Jsc of the devices-IV is slightly lower than that of the devices-III, for the well insulating properties of P(VDF-TrFE), injuring the internal charge transfer of the devices. But after all due to the less amount of P(VDF-TrFE) added in $MAPbI_3$, the detriment of Jsc decreases is slight. Compared with the devices-II, the FF of the devices-IV is slightly lower, but the decrease is not significant, indicating that the introduction of the P(VDF-TrFE) interfacial layer does not worsen the interfacial contact of the devices. In a comprehensive comparison, the devices-IV has the optimal performance parameters, thus proving that the structure constructed here can indeed improve the devices performance.

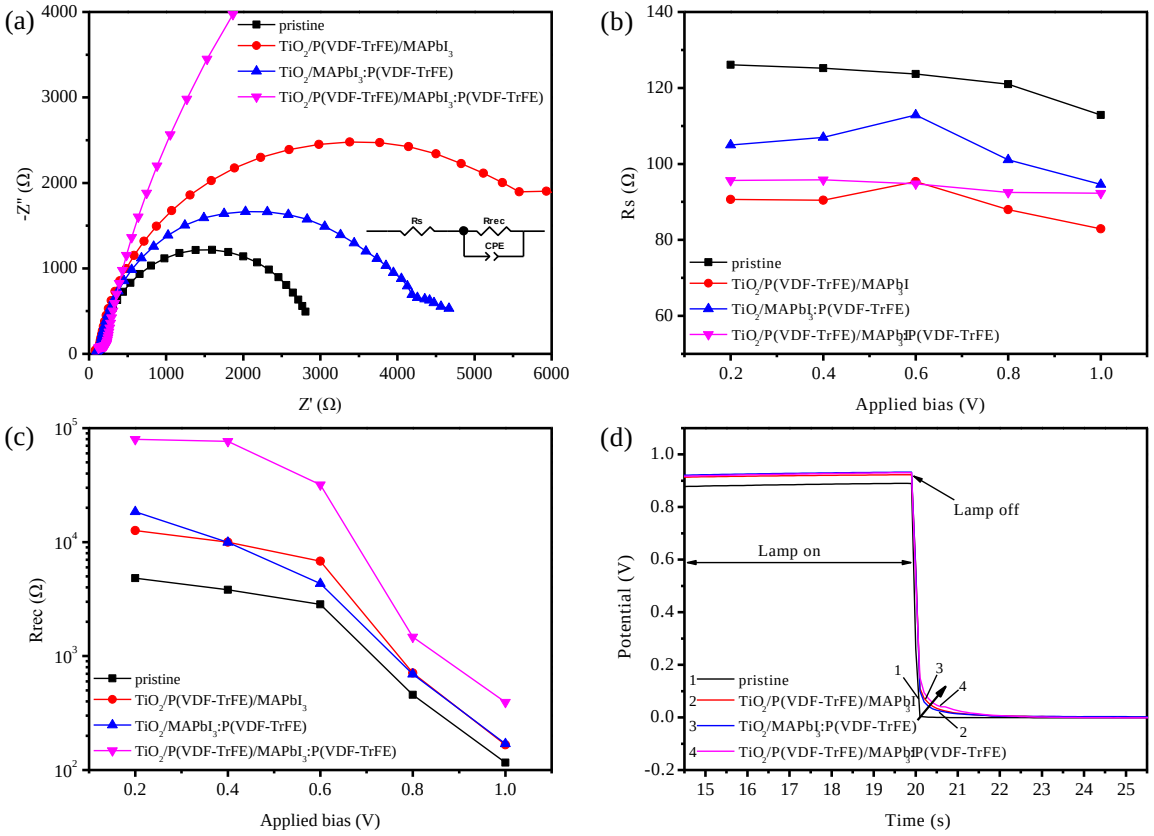

Fig. 3. a-d) EIS Nyquist plots, Series resistance (Rs) and Recombination resistance (Rrec) at different applied bias, OCVD curves of the C-PSCs based on the TiO_2/$MAPbI_3$, TiO_2/$MAPbI_3$:P(VDF-TrFE), TiO_2/P(VDF-TrFE)/$MAPbI_3$ and TiO_2/P(VDF-TrFE)/ $MAPbI_3$:P(VDF-TrFE).

In order to investigate the effect of P(VDF-TrFE) on carriers' transport and recombination at the interface, electrochemical impedance spectroscopy (EIS) of devices with different structures is measured. The Nyquist curve is fitted by the equivalent circuit in Fig.3.a to obtain the series resistance (Rs) relating to the carrier transport and the composite resistance (Rrec) reflecting the carrier complexation at the interface between the electron transport layer and the light absorb layer at different bias voltages [2,25,26]. From Fig.3.b, all the devices with P(VDF-TrFE) obtain lower Rs than the original ones, and the devices-III has the lowest Rs in the tested range, indicating a small internal carrier transport resistance and a higher Jsc. The Rs of devices-IV is between that of devices-II and devices-III, which exactly reflects that the insulating property of P(VDF-TrFE) leads to the increase of Rs inside the devices, thus decreasing Jsc. As Fig.3.c shows, the Rrec of all the devices with P(VDF-TrFE) is higher than the pristine one, and The devices-IV has the largest Rrec in the tested range, indicating that the composite resistance of the devices is enhanced to a greater extent under the dual passivation effect of P(VDF-TrFE) doping and P(VDF-TrFE) interfacial layer, which suppresses the internal carrier composite, reduces the non-radiative composite and composite loss, definitively contributes to the enhancement of Voc. Fig.3.d shows the photovoltage decay curve, the devices-IV exhibits a slower photovoltage decay trend after the light source turned off, indicating that the devices-IV has longer internal carrier lifetime, smaller

defect state density, and less carrier complexation, which is consistent with the above statistical results.

For the purpose of furtherly improving the devices performance, polarization treatments have been applied. Firstly, the effect of polarization treatment on the performance of the devices with different structure is investigated, whose direction of the applied electric field is directed from the top electrode of the FTO to the base of the sample FTO. For devices-II (Fig.4.b), the polarization treatment slightly increases the devices performance. However, the devices performance tended to decrease slightly while the polarization voltage >10 V, and the Jsc gradually decreases with the increase of the applied bias voltage. The applied voltage is also applied to P(VDF-TrFE)/$MAPbI_3$ films (Fig.4.b), it is obvious that the Jsc of devices-III has been enhanced with the increase of the polarization voltage, and the devices perform best when the polarization voltage achieves 20 V (Fig.4.c), proving that after polarization treatment the P(VDF-TrFE) interfacial layer can contribute to the enhancement of devices performance.

Finally, the polarization treatment is applied for the devices-IV (Fig.4.a) and the devices acquires the best performance (0.936 V, 16.25 mA/cm^2, 51.47% and 7.83%.) when the polarization voltage is 30 V. The enlarged graph of the red area shows the variation of the devices' Jsc with different polarization voltage, and it can be found that whit the polarization voltage increases, Jsc increases, which similar to the device-III, becomes one of the main reasons for the improvement of devices performance.

The Jsc of the C-PSCs based on the TiO_2/P(VDF-TrFE)/$MAPbI_3$ before and after polarization treatment is counted in Fig.4.b, which shows that Jsc increases with the introduction of P(VDF-TrFE) interfacial layer, and further increases after the polarization treatment (Voc also undergoes similarly). Therefore, it can be speculated that the directional arrangement of P(VDF-TrFE) dipoles inside the devices generates depolarization electric field and enhances the built-in electric field of the devices after polarization treatment, thus contributing to the separation and extraction of photo-generated carriers.

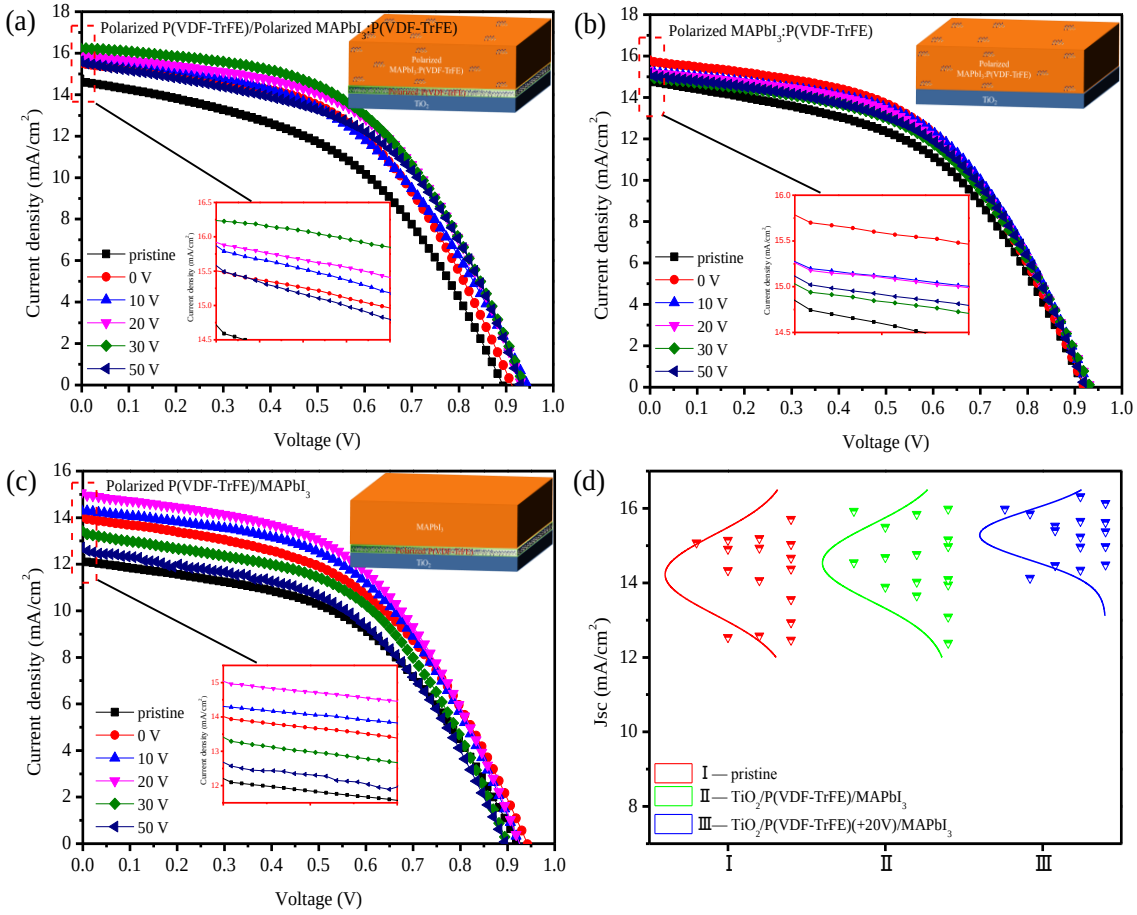

Fig. 4. a-c) J-V curves in the C-PSCs based on the TiO_2/P(VDF-TrFE)/$MAPbI_3$:P(VDF-TrFE), TiO_2/$MAPbI_3$:P(VDF-TrFE) and TiO_2/P(VDF-TrFE)/$MAPbI_3$ dependent on varied polarization voltage. d) The statistic Jsc of the C-PSCs based on the TiO_2/P(VDF-TrFE)/$MAPbI_3$ before and after polarization treatment.

So as to verify the speculation above, EQE tests are first performed on C-PSCs before and after the polarization treatment of the P(VDF-TrFE) interface layer, as shown in Fig.5.a. The EQE values of the polarization-treated devices in the test range increased significantly, indicating that the devices can collect more photogenerated electrons under the same incident light conditions, thus confirming that the enhancement of Jsc is closely related to the improvement of photogenerated electron transport, which indicates the driving force of the carrier transport between TiO_2/$MAPbI_3$ interface have been enhanced after polarization treatment.

Subsequently, Mott-Schottky tests were performed on the devices before and after polarization as a way to study the variation of the built-in electric field (recorded as V_{bi}) inside the devices [27,28], as shown in Fig.5.b.

$$\frac{1}{C^2} = \frac{2}{q\varepsilon\varepsilon_0 NA^2}\left(V - V_{bi} - \frac{KT}{q}\right) \quad (1)$$

$$w = \sqrt{\frac{2\varepsilon\varepsilon_0 V_{bi}}{eN}} \quad (2)$$

The equation (1) is used to fit the data (C: the spatial capacitance; ε: the dielectric constant; ε_0: the vacuum dielectric constant; N: the carrier concentration; A: the effective area; V: the applied bias; V_{bi}: the built-in electric field; K: the Boltzman constant; T: the absolute temperature; and q: the meta-charge), and a tangent line is made to the longest straight part of the Mott-Schottky curve (shown as a dashed line in the Fig.5.b). It is known from the equation that the slope of the tangent line is inversely proportional to the carrier concentration, and the intersection of the tangent line and the X-axis can then be calculated for the internal electric field. The data fit shows that the slope of the tangent line of the $1/C^2$-V curve of the devices changes from $-2.77 \cdot 10^{15}$(before polarization) to $-4.34 \cdot 10^{15}$ (after polarization), and the slope $k=2/(q\varepsilon\varepsilon_0 NA^2)$ shows that the devices has a lower carrier concentration after polarization treatment, which is more favorable to the transport of photogenerated electrons. Meanwhile, the calculated results show that the built-in electric field of the devices before and after the polarization treatment is 0.807 V and 0.832 V respectively, indicating that the polarization treatment of the P(VDF-TrFE) interface layer helps to enhance the built-in electric field inside the devices, which promotes photogenerated carrier separation and suppresses carrier complexation [29].

The depletion layer width (recorded as w), calculated by the equation (2), is another general index to characterize the carrier transport performance. The calculation results show that the w of the devices increases from 130 nm to 165 nm after the polarization treatment of the P(VDF-TrFE) interfacial layer, which indicates that the polarization treatment results in the increase of the dipole width from directional depolarization electric field generated by the directional alignment of the dipole [30], and promotes photogenerated electron transport.

In order to rule out that the enhancement effect of polarization treatment on the devices is from the TiO_2 layer rather than the P(VDF-TrFE) interface layer. As the Fig.5.c and 5.d shows, polarization of the TiO_2/$MAPbI_3$ reveals that the PCE and the electric field built of the devices are almost unchanged before and after polarization, so this speculation can be excluded.

Therefore, it can be inferred that the dipole inside the P(VDF-TrFE) interface layer under the action of the polarization electric field will arrange directionally to produce a directional depolarization electric field, which increases the built-in electric field and depletion layer width w of the devices, enhances the carrier transport driving force, promotes the transport of photogenerated electrons inside the devices, increases the EQE value and Jsc, and finally improves the devices performance, which is consistent with the conclusion that the reduction of series resistance Rs and improvement of the Jsc.

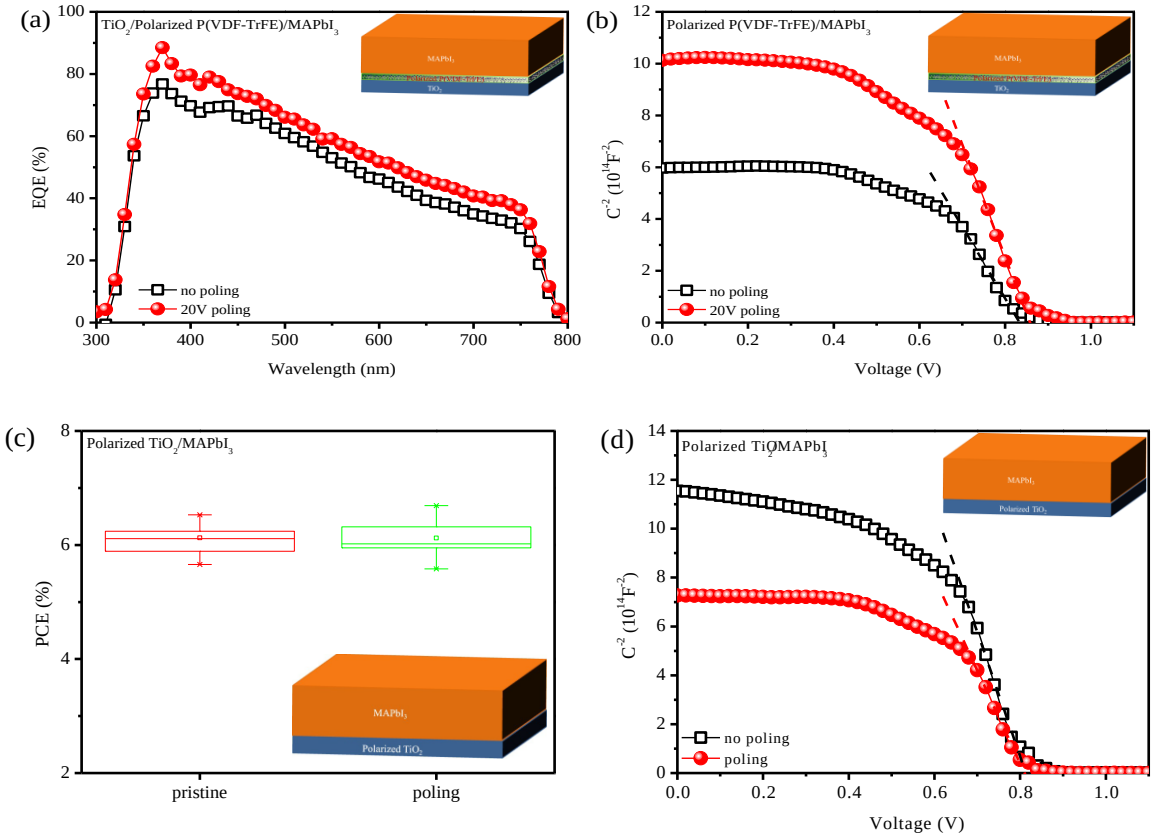

Fig. 5. a, b) EQE spectra and $1/C^2$ versus applied voltage plots of the C-PSCs based on the TiO_2/P(VDF-TrFE)/$MAPbI_3$ before and after polarization treatment. c, d) The statistic PCE and $1/C^2$ versus applied voltage plots of the C-PSCs based on the TiO_2/$MAPbI_3$ before and after polarization treatment.

Is it enough to only polarize the P(VDF-TrFE) interface layer? As the Fig.6.a shows, the effect of different degrees of polarization treatment of P(VDF-TrFE)/$MAPbI_3$:P(VDF-TrFE) on the performance of the device is studied. It can be found that polarization can improve the performance of the devices, and the best performance can be achieved for the overall polarization of devices-IV.

In addition, the influence of polarization treatment on the hysteresis effect of the device has been explored. It is clear that the variation of hysteresis factor is inversely proportional to that one of the built-in electric field with the polarization voltage from Fig.6.b. One of the main reasons for the hysteresis phenomenon is ion migration, which can lead to a weakening of the built-in electric field of the devices, leading to the accumulation of charge at the carrier transport layer/photoabsorption layer interface and generates hysteresis [31-33]. From the above analysis, the main reason for the devices performance enhancement is that the depolarization electric field generated by the P(VDF-TrFE) interface layer enhances the built-in electric field, which promotes the separation and transport of photogenerated carriers at the TiO_2/$MAPbI_3$ interface (as shown in Fig.1) and reduces the interfacial charge accumulation, reducing the hysteresis effect.

For the sake of further prove that the carrier transport of the device has been improved after polarization treatment, the variation of Rs with applied voltage and the capacitance frequency

curve of the devices before and after polarization treatment have been tested. As the Fig.6.c show, the polarization-treated devices have lower Rs, indicating that the polarization treatment reduces the charge transport resistance and promotes the transport of photogenerated electrons from the $MAPbI_3$ layer to the TiO_2 layer, which is consistent with the performance enhancement caused by the enhanced electric field built into the devices after polarization as described above. From the capacitance frequency curves (Fig.6.d), the polarization treatment provides devices with lower capacitance response, indicating that polarization treatment can reduce the electrode polarization of the devices and reduce the interfacial charge accumulation, which is beneficial to suppress the hysteresis effect [34].

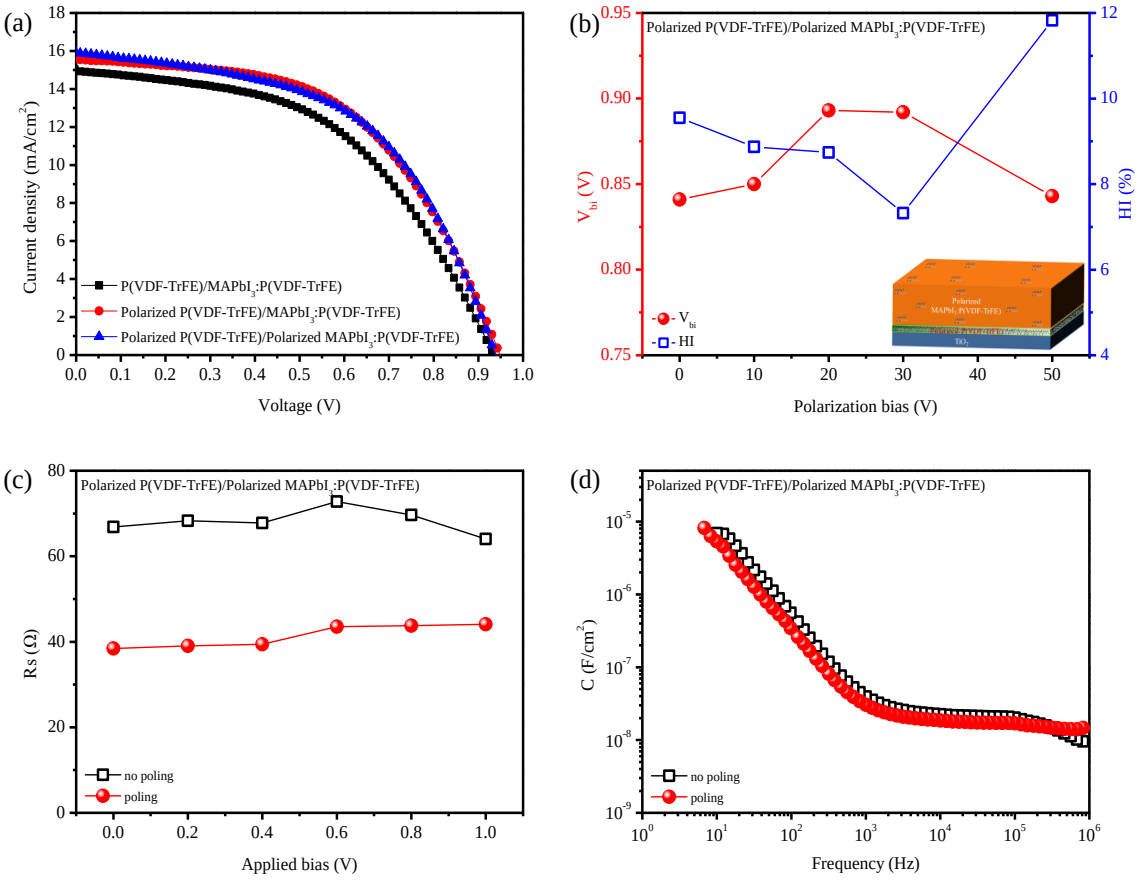

Fig. 6. a) J-V curves in the C-PSCs based on the P(VDF-TrFE)/$MAPbI_3$:P(VDF-TrFE), Polarized P(VDF-TrFE)/$MAPbI_3$:P(VDF-TrFE) and Polarized P(VDF-TrFE)/Polarized $MAPbI_3$:P(VDF-TrFE). b) Curves of build-in field (V_{bi}) and hysteresis index (HI) dependent on varied polarization voltage. c, d) Rs at different applied bias and C-f curves of the C-PSCs based on the P(VDF-TrFE)/$MAPbI_3$:P(VDF-TrFE) before and after polarization treatment.

4. Conclusion

In summary, this work introduces organic ferroelectric P(VDF-TrFE) into C-PSCs, aiming to effectively promote the separation and transport of carriers at TiO_2/$CH_3NH_3PbI_3$ interface. The structure of FTO/TiO_2/P(VDF-TrFE)/$CH_3NH_3PbI_3$:P(VDF-TrFE)/C is built successfully. On the

one hand, the additive P(VDF-TrFE) can improve the quality of perovskite film, which decreases internal defects and suppresses the carriers' recombination. One the other hand, P(VDF-TrFE) interface dipole layer is inserted into TiO_2/$CH_3NH_3PbI_3$:P(VDF-TrFE) interface after polarization treatment. The built-in field in C-PSCs is enhanced as well as the force for photo-electron transport at interface. Finally, the prepared C-PSCs obtains a high PCE of 7.83% with an excellent Jsc of 16.25 mA/cm^2. And the hysteresis is reduced as well. This simple and feasible method will be helpful to the commercialization of C-PSCs in the future.

Acknowledgements

This work was supported by the Fundamental Research Funds for the Central Universities (No. NS2020038). A Project Funded by the Priority Academic Program Development of Jiangsu Higher Education Institutions.

References

[1] H. Chen, S. Yang, J. Mater. Chem. A. 7, 15476 (2019) https://doi.org/10.1039/C9TA04707G
[2] Y. L. Yang, Z. H. Liu, W. K. Ng et al, Adv. Funct. Mater. 29, 1806506 (2018) https://doi.org/10.1002/adfm.201806506
[3] NREL Best Research-Cell Efficiency Chart, https://www.nrel.gov/pv/cell-efficiency.html.
[4] H. Meng, J. Zhou, J. Hou et al, Advanced Materials, 30(21) 1706975 (2018) https://doi.org/10.1002/adma.201706975
[5] H. J. Snaith, A. Abate, J. M. Ball et al, The journal of physical chemistry letters, 5(9) 1511 (2014). https://doi.org/10.1021/jz500113x
[6] J. Hu, R. Gottesman, L. Gouda et al, ACS Energy Letters, 2(5) 950 (2017) https://doi.org/10.1021/acsenergylett.7b00212
[7] B. Roose, S. Pathak, U. Steiner, Chemical Society Reviews, 44 8326 (2015). https://doi.org/10.1039/C5CS00352K
[8] Y. Xiao, C. Wang, K. K. Kondamareddy et al, ACS Applied Energy Materials, **1**(10) 5453 (2018).
[9] Y. Rong, Z. Ku, A. Mei et al, The journal of physical chemistry letters, 5(12) 2160 (2014). https://doi.org/10.1021/jz500833z
[10] M. Li, Y. Huan, X. Yan et al, ChemSusChem, 11(1) 171 (2018). https://doi.org/10.1002/cssc.201701911
[11] S. F. Shaikh, H. C. Kwon, W. Yang et al, Jouranl of Materials Chemistry A, 4 15478 (2016). https://doi.org/10.1039/C6TA05008E
[12] Y. H. Lee, J. Luo, M. K. Son et al, Advanced Materials, 28 3966 (2016) https://doi.org/10.1002/adma.201505140
[13] L. F. Liu, A. Y. Mei, T. F. Liu et al, Journal of the American Chemical Society, 137(5) 1790 (2015). https://doi.org/10.1021/ja5125594
[14] M. Y. Zhang, Q. Chen, R. M. Xue et al, Nature communications, 10(1) 4593 (2019) mhttps://doi.org/10.1038/s41467-019-08642-y
[15] Y. B. Yuan, T. J. Reece, P. Sharma et al, Nature Materials, 10 296 (2011). https://doi.org/10.1038/nmat2951

[16] B. Yang, Y. B. Yuan, P. Sharma et al, Advanced Materials, 24(11) 1455 (2012)
https://doi.org/10.1002/adma.201104509
[17] Z. G. Xiao, Q. F. Dong, P. Sharma et al, Advanced Energy Materials, 3(12) 1581 (2013).
https://doi.org/10.1002/aenm.201300396
[18] I. Pintilie, V. Stancu, A. Tomulescu et al, Materials & Design, 135 112 (2017).
https://doi.org/10.1016/j.matdes.2017.09.013
[19] A. Pérez-Tomas, H. B. Xie, Z. W. Wang et al, Sustainable Energy Fuels, 3(2) 382 (2019).
https://doi.org/10.1039/C8SE00451J
[20] M. Z. Wang, H. J. Feng, C. X. Qian et al, Advanced Functional Materials, 29(1) 1806427 (2018).
https://doi.org/10.1002/adfm.201806427
[21] Y. L. Yang, Z. H. Liu, W. K. Ng et al, Adv. Funct. Mater, 29 1806506 (2018)
https://doi.org/10.1002/adfm.201806506
[22] C. C. Zhang, Z. K. Wang, S. Yuan et al, Advanced Materials, 31(30) 1902222 (2019)
https://doi.org/10.1002/adma.201902222
[23] E. D. Jia, D. Wei, P. Cui et al, Advanced Science, 6(16) 1900252 (2019)
https://doi.org/10.1002/advs.201900252
[24] Y. Xiao, G. Han, Y. Li et al, Journal of Materials Chemistry A, 2 16856 (2014)
https://doi.org/10.1039/C4TA03658A
[25] X. B. Xu, Z. H. Liu, Z. X. Zuo et al, Nano Letters, 15 2402 (2015)
https://doi.org/10.1021/nl504701y
[26] I. Zarazua, G. F. Han, P. P. Boix et al, The Journal of Physical Chemistry Letters, 7 5105 (2016)
https://doi.org/10.1021/acs.jpclett.6b02193
[27] K. M. O'Malley, C. Z. Li, H. L. Yip et al, Advanced Energy Materials 2 82 (2012)
https://doi.org/10.1002/aenm.201100522
[28] W. A. Laban, L. Etgar, Energy & Environmental Science, 6 3249 (2012).
https://doi.org/10.1039/c3ee42282h
[29] W. Peng, L. F. Wang, B. Murali et al, Advanced Materials, 28 3383 (2016)
https://doi.org/10.1002/adma.201506292
[30] K. Wojciechowski, M. Saliba, T. Leijtens et al, Energy & Environmental Science, 7 1142 (2014).
https://doi.org/10.1039/C3EE43707H
[31] Y. C. Shao, Z. G. Xiao, C. Bi et al, Nature Communications, 5 5784 (2014).
https://doi.org/10.1038/ncomms6784
[32] S. V. Reenen, M. Kemerink, H. J. Snaith, The Journal of Physical Chemistry Letters, 6 3808 (2015).
https://doi.org/10.1021/acs.jpclett.5b01645
[33] J. J. Shi, H. Y. Zhang, X. Xu et al, Small, 12 5288 (2016).
https://doi.org/10.1002/smll.201601543
[34] H. S. Kim, I. H. Jang, N. Ahn et al, The Journal of Physical Chemistry Letters, 6 4633 (2015).
https://doi.org/10.1021/acs.jpclett.5b02273